Acta Geologica Sinica (English Edition), 2020, 94(1): 103–113

The Environment Significance of Aerinite — First Discovered in the UBC Cliffs

WANG Guanyu and WANG Hejing*

School of Earth and Space Sciences, Peking University, Beijing 100871, China

Abstract: To analyze the composition and structure of the pale blue outcrop from the UBC Cliffs and research the environmental significance of aerinite recorded in the sediments, mineral composition, bulk chemical composition and structural analyses were carried out by means of X-ray diffraction (XRD), field emission scanning electron microscope (FESEM), transmission electron microscope (TEM), electron microprobe analysis (EMPA) and X-ray fluorescence spectra (XRF). Quartz, feldspar, mica, chlorite and aerinite as well as a small amount of amphibole, calcite, clinopyroxene, rutile, perovskite and apatite are recorded in the sediments. It is reported for the first time that the aerinite occurs in a high latitude area and in sediments paragenetic with mica and chlorite. The large span in grain size shows a typical characteristic of fluvioglacial sediments. Geochemistry characteristics (CIA, CIW, PIA, WIP and ICV) verify that there is virtually no chemical weathering. Mineralogy and geochemistry features of the UBC Cliffs sediments indicate that aerinite is accommodate to the high latitude and cold, dry climate. As the sediments show high similarity to those of their provenance, they have great significance in the identification of the forming condition and origin of the aerinite.

Key words: UBC Cliffs, sediments, aerinite, muscovite, chlorite, environment significance

Citation: Wang et al., 2020. The Environment Significance of Aerinite — First Discovered in the UBC Cliffs. Acta Geologica Sinica (English Edition), 94(1): 103–113. DOI: 10.1111/1755-6724.14402

1 Introduction

The UBC (University of British Columbia) Cliffs locates in the Fraser River delta, adjacent to the University of British Columbia. The Fraser River delta, south of Vancouver, is an important agricultural, fishery and industry area on the west coast of Canada. However, because of the constant tidal washout, the cliffs are now suffering from sustained corrosion. From the end of the last century, deforestation started due to the construction of the new university and defense works, which accelerates the erosion of the UBC Cliffs. It is at present an impending work to protect and reconstruct the UBC Cliffs for its threat to surrounding constructions. So, fundamental research of this area is of crucial significance. Moreover, sediments outcropping here show uncommon light blue, which arouses the authors' interest. Previous studies of the area focused on deposit, transport process, erosion rates and deposit of the delta (Attard et al., 2014; Clague et al., 1991; Clague et al., 1983; Lintern et al., 2016); diagenetic cementation of sands (Garrison et al., 1969); the relationship between sediments and aquatic animals, plants and microorganisms (Yin et al., 2016); the determination of exact depositional position (La Croix and Dashtgard, 2015). However, no one has reported such light blue mineral aerinite.

The word "aerinite" was first described by Von Lasaulx in 1876 (who named it after the Greek word "aerinos" for blue). It was included by Groth (1898) as a mixture of silicates and iron hydroxides in his mineralogical tables. Casas and Llopis (1992), Salvadó et al. (2008), Clark et al. (2010) and Pérez-Arantegui et al. (2013) studied the blue pigment in the Romanesque frescoes of the Pyrenean region, and asserted that aerinite was the raw material used in the blue pigment. Further study showed it has relatively high thermal stability and good to very good resistance to air pollutants like chemicals, heat and light. The thermal behavior of aerinite was observed by Daniel et al. (2008) and Ibáñez-Insa et al. (2012). It was verified that aerinite chromatic properties are influenced by dehydration. Specifically, aerinite is totally degraded above 400°C, then it recrystallizes into Fe-rich augite at 800° C, and eventually transforms to hematite and plagioclase at 1000° C, with the chromatic of aerinite undergoing blue, greenish (400°C), yellowish-brown (600°C) and brownish -red (1000°C). Above researches might provide useful information regarding the original state of a painting damaged by a fire event. Since the last century, lots of French and Spanish researchers have studied the structure of aerinite and confirmed that aerinite is effectively a new mineral. The structure of aerinite was determined by Rius et al. (2004), Rius et al. (2009) and Frost et al. (2015) as a fibrous silicate containing carbonate in a large channel. There is an inherent mineralogical interest on it because of its striking blue color and its unusual composition containing both silicate and carbonate units. Such blue fibrous mineral is usually associated with the alteration of subvolcanic rocks (dolerites and diabases) (Rius et al., 2009) or mafic igneous rocks (Ibáñez-Insa et al., 2012) in the southern Pyrenees. It has also been found in Andalusia

* Corresponding author. E-mail: hjwang@pku.edu.cn

and Marocco. Aerinite as inclusion in blue quartz occurs in ophite near Malaga Spain, which is the only area known to have produced crystals colored by aerinite (Silva, 1996). It is also reported as inclusion in Odisha's beryl (emerald) sample (Jena and Mishra, 2017) and plagioclase (Lu et al., 2016). Generally associated with prehnite, scolecite, mesolite, quartz, feldspar (microcline, plagioclase) and pyroxene, aerinite has never been reported in Vancouver, nor had anyone referred to its paragenesis with chlorite and mica in sediments.

The aim of the present study is to analyze the composition and structure of the pale blue outcrop from the UBC Cliffs and research the environment significance of aerinite recorded in the sediments via mineralogical and geochemistry methods. Such interest is due to its geological importance for unusual composition and uncommon outcrop worldwide and its artistic and economic importance as an excellent natural blue mineral pigment.

2 Geologic Setting

The sediments sample was collected from the UBC Cliffs (Point Grey Cliffs, 49°15'N, 123°15'W，see Fig. 1) in Vancouver, Canada. Point Grey is an upland area of Vancouver underlain principally by unconsolidated deposits associated with the Pleistocene glaciation, which is now the Fraser River estuary. South to Vancouver, the Fraser River delta is the largest and most important delta on the west coast of Canada. It has formed since the disappearance of the Cordilleran ice sheet, and then it was gradually overlain by fine grained and sandy sediments derived from various volcanic, plutonic and sedimentary rocks (Amos et al., 1997; Hart et al., 1998). The UBC Cliffs lie west of the Fraser River, belonging to the beach-cliff system in Vancouver, where is quite different from the nearby Fraser River delta (Clague and Bornhold, 1980). Previously referred to as "Quadra Group" and "Point Gray Formation", it is now described uniformly as "Quadra Sand". The term "Quadra Sand", changing with time for an extended period of time, is controversial. Now the most widely accepted definition, proposed by Clague (1976) and Clague (1977), is namely "the glaciofluvial outwash derived mainly from weathering of granitic rock in the southern Coast Mountains", which is horizontally stratified, containing quartz, feldspar and lithic fragments

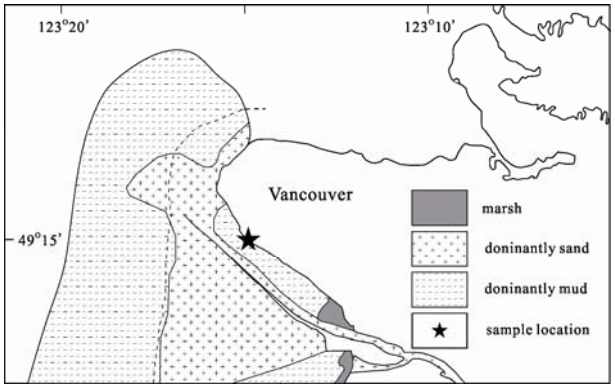

Fig. 1. A sketch map of the studied area (after Luternauer, 1980).

(Armstrong and Clague, 1977; Armstrong et al., 1965; Clague et al., 2005; Mathewes, 1979; Ryder et al., 1991). During the last ice age, glaciers from the north covered the sedimentary deposits, and these hundreds of feet thick glaciers compressed the underlying sand and sedimentary deposits. Then following the warming trend 10 to 15 thousand years ago, the land takes on the view known as "Point Grey" now. North facing sea cliffs at Point Grey, formed largely with horizontally stratified, well sorted sand and silt, are experiencing severe erosion which brings serious threat to nearby constructions. The land in this area is composed of a top layer of slowly permeable fluvioglacial till underlain by a porous but very stable layer of Quadra Sand, through which are thin layers of clay that are also slowly pervious. One of these clay layers can be seen at the north end of the cliffs at an elevation of about 20 meters.

3 Material and Methods

The sediments sample was slightly grinded and ultrasonic dispersed. After precipitation for two hours, 2 cm supernate was taken and numbered Aer-3 (according to the Stokes' Law, the particle-size was calculated at <1.8 μm). Then stirred the remaining sample and precipitated for four hours, and numbered the 2 cm supernate Aer-1 (<1.2 μm) and the remaining portion Aer-2 (>1.2 μm). The sample for TEM was suspended in alcohol and ultrasonicated to further disperse. A drop of the suspension was then placed on a copper mesh coated with a carbon film (Wang et al., 2014). XRD, SEM, TEM, EMPA and XRF analyses were performed for whole rock, Aer-1, Aer-2 and Aer-3. XRD patterns were collected by using an X'Pert Pro MPD diffractometer with an X'Celerator detector. The measuring conditions of XRD were Cu Kα radiation (λ=0.154056 nm), 40 kV and 40 mA, 5–90° (2θ) scanning range, 0.017° (2θ) step size (Wang et al., 2002). Deconvolution technique (Highscore Plus, version 4.6) was used to extract the structural data of aerinite with reliabilities all below 2%. The Rietveld refinement was performed to quantify relative percentage of minerals in the sediment, in which whole-pattern fitting was carried out. The structure of aerinite was refined using software DIFFRAC.SUITE TOPAS 5 and the pseudo-Voigt function was used for peak fitting. Field emission scanning electron microscope (FESEM) measurement was performed with a QUANTA-650FEG microscope operating at 15 kV, beam spot diameter 4.0 μm. Size distribution was measured by a Mastersizer 2000 instrument at 20°C, 2400 r/min. Chemical composition was obtained by a ADVANT`XP+ X-ray fluorescence spectrometer (XRF) and by a JXA-8230 electron microprobe analysis (EMPA) at 15 kV and 10^{-8} A, beam spot diameter 1 μm (Li et al., 2017). Transmission electron microscope was performed with a JEM-2100 Field emission high resolution transmission electron microscope at 200 kV.

4 Results and Analyses

4.1 XRD analysis

XRD patterns indicate that quartz, plagioclase chlorite,

mica, aerinite and a small amount of amphibole and calcite are presented in the sediments. The phase identification and semi-quantitative analysis results are summarized in Figs. 2 and 3. As illustrated in Fig. 3, plagioclase is the major mineral of the four specimens (over 70%), followed by quartz, chlorite, mica and aerinite. Plagioclase content of the four samples shows little change, indicating a quite large granularity span, while calcite teeming only in the finer Aer-1 attests its fine particle size. The fact that amphibole is almost absent in Aer-1, where the proportion of calcite increases, shows amphibole is coarser than calcite in size. The highest content of aerinite emerges in the whole rock, then in Aer-3 and Aer-1, however, it is hardly detected in Aer-2.

4.2 Particle size distribution

Particle size is a basic parameter describing sediment distribution characteristic, which acts as a leading indicator to identify deposit environment, invert and deduce transport and deposition mode. As a result of the joint actions of provenance, hydrodynamic force, motion distance and terrain, such a parameter offers an effective probing to the provenance and hydrodynamic conditions, and help to reconstruct ancient geological history.

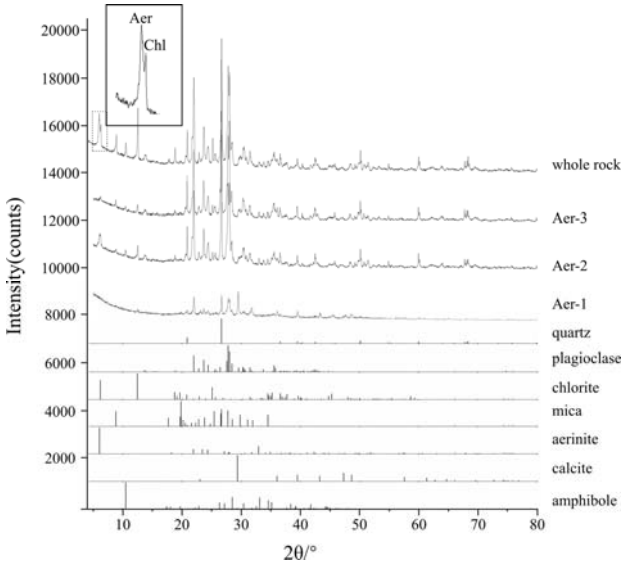

Fig. 2. XRD patterns of the sediments.
The figure shows the XRD pattern of quartz, plagioclase, chlorite (Chl), mica, aerinite (Aer), calcite and amphibole, and the existence of above minerals in the sediments.

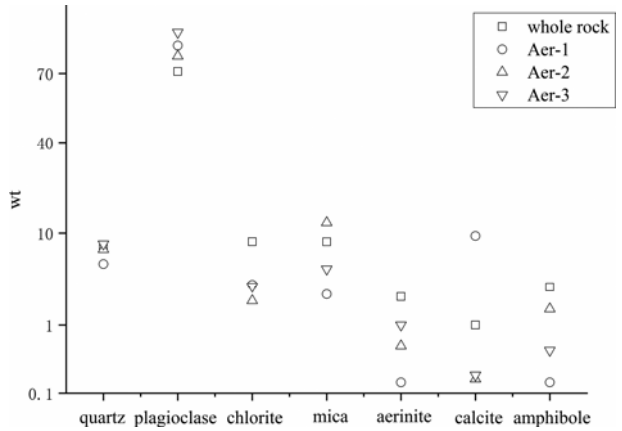

Fig. 3. Relative percentage of higher concentration minerals in the sediments (not including clinopyroxene, rutile, perovskite and apatite).

Accumulation of different grain sizes can be seen from 0.74 to 11.2 φ (Fig. 4), which conforms to the wide particle size distribution range of fluvioglacial sediments. The curve approximates the normal distribution, with a little peak in small size interval. It peaks at about 6 φ, indicating the maximum content falling on fine silt, which is an evidence of weaker hydrodynamic condition and a comparatively stable hydrological environment. From the probability cumulative grain size curve, a small amount of bed load and saltation load can be seen accounting for a proportion of 0.7% and 2%, respectively, and suspended load takes up the rest. The suspended load consists of three comparatively steep parts, among which the rather shaper one above 10 φ is due to the inherent abrasion of glaciation.

According to Folk et al. (1970)'s textural classification of gravel-free sediments and sedimentary rocks, sediments from the UBC Cliffs are silt dominated (Table 1). Other parameters are also summarized in Table 2. Mean grain size (φ), sorting, skewness and kurtosis coefficients are calculated and graded by using moment method

Table 1 Relative percentage of higher concentration (>1%) minerals in the sediments (wt%±standard deviation, not including clinopyroxene, rutile, perovskite and apatite)

Mineral	Whole-rock	Aer-1	Aer-2	Aer-3
Quartz	7.28±1.14	5.14±0.98	7.14±1.04	8.02±1.58
Plagioclase	70.76±3.05	79.90±2.19	76.39±3.08	83.78±1.48
Chlorite	8.41±1.92	3.10±0.47	2.01±0.48	2.98±1.14
Mica	8.39±2.28	2.41±0.79	12.27±1.30	4.57±1.52
Aerinite	2.25±1.58	–	–	1.00±0.83
Calcite	1.00±0.96	9.45±2.19	–	–
Amphibole	2.91±1.10	–	1.60±1.02	–

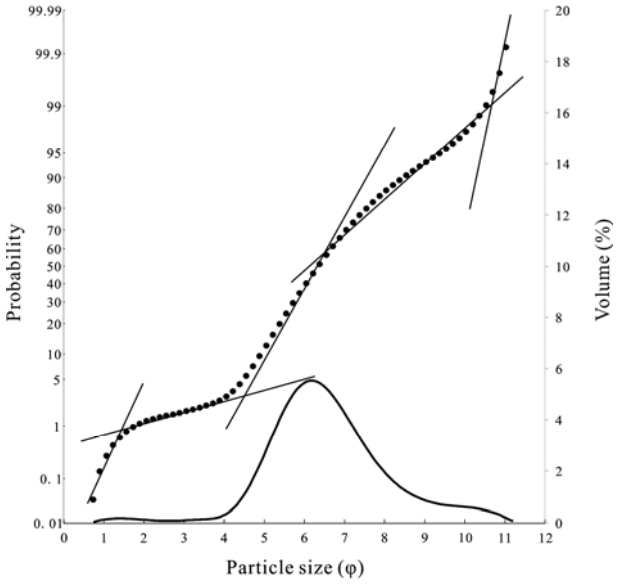

Fig. 4. Particle size distribution and probability cumulative grain size curve of the sediments.

(McManus, 1988). Medium to very fine silt dominates the sediments with a percentage of 75.05% and the content of clays is 15.45%. Generally, it has a relatively large content span of all particle sizes with a poor sorting coefficient than sediments from beach and rivers, and a skewness coefficient around zero.

Above results show a typical figure of fluvioglacial sediments. As such stable hydrological environment can preserve a massive of argillaceous sediment, it can act as a trace of the provenance.

As shown in Fig. 5a, randomly distributed granular mineral particles are loosely packed, with schistose and prismatic minerals filling in the interstice, and arrow indicating bio-organic matters. Large and small particles packed together. SEM images and EDS results (Table 3) demonstrate that granulated particles (principally quartz and feldspar, Fig. 5b) show the highest content, with a diameter varying from several micrometers to several

Table 2 Data of particle size distribution of the sediments

Millimeters (mm)	Phi (φ)	Content (%)	Wentworth size class (Wentworth, 1922)	Folk size class (Folk et al., 1970)
1–0.5	0–1	0.14	coarse sand	
0.5–0.25	1–2	0.96	medium sand	sand
0.25–0.125	2–3	0.54	fine sand	
0.125–0.0625	3–4	0.88	very fine sand	
0.0625–0.031	4–5	6.98	coarse silt	
0.031–0.0156	5–6	25.26	medium silt	silt
0.0156–0.0078	6–7	31.13	fine silt	
0.0078–0.0039	7–8	18.66	very fine silt	
< 0.0039	> 8	15.45		clay

Other particle size parameters of the sediments			
	Value	Grading	Standard scale (McManus, 1988)
Mean grain size (φ)	6.58	fine silt	6–7
Sorting coefficient	1.52	relatively poor	1–2
Skewness coefficient	0.14	symmetrical	–0.33–0.33
Kurtosis coefficient	4.45	very platy kurtic	2.75–4.50

Table 3 chemical composition of the sediments

EDS (SEM) results of the sediments (wt%)									
	O K	Na K	Mg K	Al K	Si K	K K	Ca K	Ti K	Fe L
Aerinite	47.41	0.93	3.97	7.04	19.42	0.69	5.73		14.82
Chlorite	48.10		9.35	8.08	9.07				25.41
Chlorite	48.32		10.12	7.58	9.91				24.06
Mica	55.31	0.53		16.47	22.26	5.43			
Mica	59.83	0.96		15.55	19.01	4.65			
Mica	59.66	0.82	0.32	14.86	18.30	6.04			
Feldspar	48.38	4.35		12.97	28.44		5.86		
Feldspar	54.07	3.74		12.28	24.26		5.66		
Feldspar	57.23	3.69		12.36	21.19		5.54		
Clinopyroxene	45.47	0.87	4.37	6.44	19.47		7.76		15.62
Rutile	38.68							61.32	
Perovskite	60.84						17.78	21.37	

XRF results of the sediments (wt%)											
SiO_2	Al_2O_3	Na_2O	CaO	Fe_2O_3	MgO	K_2O	TiO_2	P_2O_5	MnO	LOI	sum
60.56	18.56	5.29	4.26	3.77	2.63	1.56	0.54	0.218	0.078	2.36	99.826

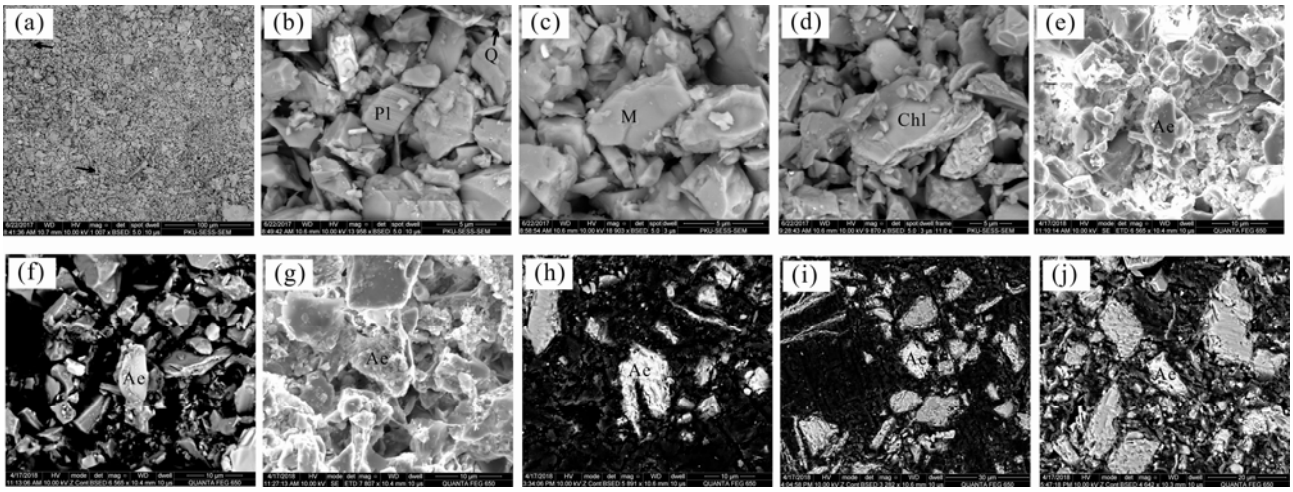

Fig. 5. SEM images of the sediments.

(a) Granular mineral particles in schistose and prismatic forms filling in the interstice; (b) granular quartz (Q) and feldspar (Pl); (c) platy mica (M); (d) chlorite (Chl); (e-j) irregular clastic particles aerinite (Ae).

dozens of micrometers. These granulated particles are almost not rounded, revealing the physical crushing under glaciation. The platy and schistose minerals are mainly mica (Fig. 5c) and chlorite (Fig. 5d), which are about 5μm in size. Bio-organic matters can also be seen (arrow in Fig. 5a). Fig. 5e-j demonstrates irregular clastic aerinite particles in size of about 5×10 μm. These aerinite particles showing in bright gray in BSED images are distinguishable from those dark gray minerals such as feldspar and clay minerals, and from the brighter apatite as well.

The EMPA data of aerinite and the calculated atomic content in the unit cell are referred to Table 4.

4.3 TEM analysis

Lump and fibrous minerals alternate in the TEM images. An HRTEM image shows two-dimensional parallel lattice fringes with a period of about 1.56 nm (Fig. 6a), which is less beam sensitive than clay minerals. SAED pattern (right top of Fig. 6a) shows it basically matches [100] or [010] of aerinite (Rius et al., 2004). Figs. 6b and 6c show some bending aerinite crystals with different lattice spacing. Fig. 6d shows a series of lattice fringes in 1 nm spacing and corresponding SAED pattern along [001]*. While Fig. 6e demonstrates a series of bending lattice fringes in 1 nm spacing, which is caused by the folding of TOT structure. Both Figs. 6d and 6e indicate the presence of mica structure. Moreover, the wider fringes in Fig. 6e are 1 nm along [001]* and the narrower 0.45 nm fringes are perpendicular to [001]*. According to mica's structure, only (010) and (0-10) planes are perpendicular to the (001) plane with an interplanar spacing of 0.45 nm, therefore, the image was taken along [100] or [-100] of mica.

Table 4 EMPA data of aerinite and calculated atomic content in the unit cell by assuming 12 (Si + Ti) atoms in the pyroxene chains

Oxide	wt(%)	Atomic contents
SiO_2	37.08	11.63
TiO_2	1.59	0.37
		∑ 12.00
Al_2O_3	13.77	5.09
Cr_2O_3	0.05	0.01
FeO*	17.06	2.67 (Fe^{3+})
		1.80 (Fe^{2+})
MnO	0.16	0.04
NiO	0.05	0.01
MgO	7.36	0.38
		∑ 10.00
MgO		3.06
CaO	1.07	0.36
Na_2O	1.03	0.63
K_2O	1.88	0.75
		∑4.80
Total	81.09	

*: total Fe

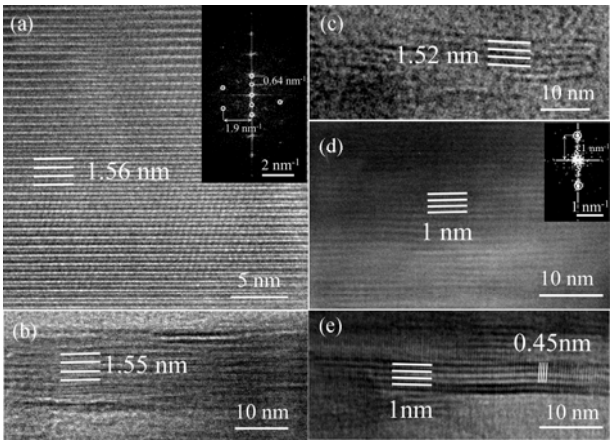

Fig. 6. TEM images of the sediments.
(a) Two-dimensional lattice fringes and corresponding SAED pattern of aerinite, showing a period of about 1.56 nm; (b-c) bending aerinite crystals with different lattice spacing; (d) a straight regular mica plane, corresponding SAED pattern showing 1 nm along [001]*; (e) bending stacked two-dimensional mica lattice fringes.

5 Discussion

Sediments from the UBC Cliffs are mainly detrital minerals, dominantly reflecting their source area and being influenced by erosion and weathering, and to a lesser degree by diagenesis. Above experimental results show aerinite and its paragenetic minerals (quartz, feldspar, chlorite, mica, amphibole, calcite, clinopyroxene, rutile, perovskite and apatite) are fundamentally in accordance with Mackintosh and Gardner (1966)'s elucidation that sediments contributed to the lower Fraser Valley are composed largely of quartz, feldspar, chlorite, mica and amphibole, while clay fractions contain montmorillonite and chlorite as the dominant minerals with lesser amounts of micaceous material, mixed-layer montmorillonite-chlorite and minor amounts of kaolin. However, his report didn't mention the pale blue mineral aerinite this essay refers to.

5.1 Aerinite chemical component and XRD data

Aerinite in the sample studied is usually irregular clastic particles in size of about 5×10 μm, which is a little different from the fibrous morphology mentioned by previous study. Such difference may be derived from a short transportation of sediment.

With respect to chemical composition, EDS results show aerinite contains elements Ca, O, Fe, Na, Mg, Al and Si (see Fig. 7), and the EMP analysis reveals that the structural formulae is of little deviation from the chemical formula given by Rius et al. (2004).

Rietveld refinement analysis (see Fig. 8) was performed to calculate the structure parameters of aerinite based on space group of *P*3*c*1 and the previously reported chemical

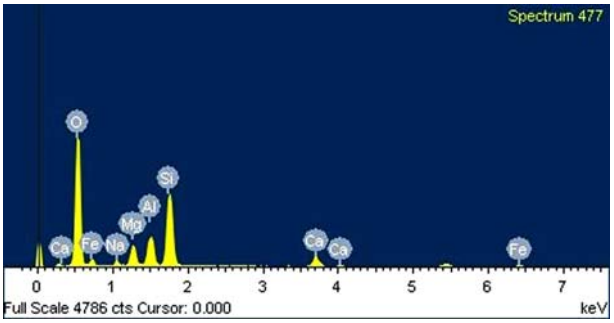

Fig. 7. Energy spectrum of aerinite.

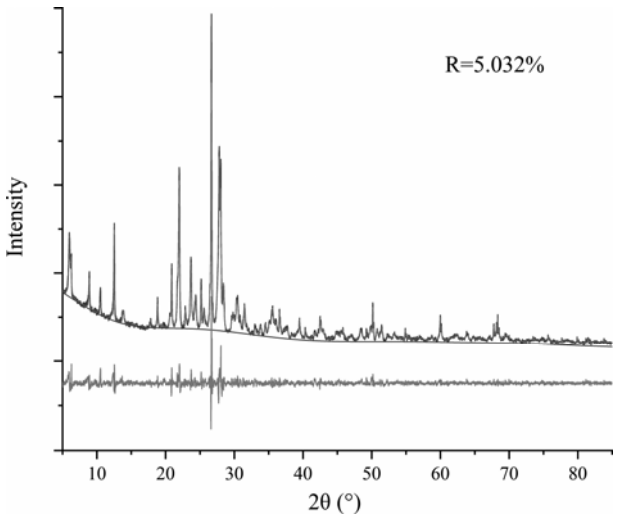

Fig. 8. Rietveld refinement of XRD pattern.
The residual between measured and calculated patterns (R factor) is listed on the top right of the image.

formula by Rius et al. (2004). Deconvoluted and measured from XRD pattern, the unit-cell parameters of aerinite are refined as a=b=1.692(5), c=0.5220(32) nm, γ=120°, which is intermediately agreed with a=b=1.68820, c=0.52251 nm, γ=120° refined by Rius et al. (2004). XRD data and fractional coordinates and occupancies for the structure are listed in Tables 5 and 6.

It can, from Table 7, see that the crystal structures of aerinite from different occurrences are in two types: one (Azambre and Monchoux, 1988) is the monoclinic crystal system, and the other (Rius et. al. 2004, 2009, and this study) belongs the trigonal crystal systems ($P3c1$). Comparing the trigonal aerinites they are almost the same with standard deviation of 0.02265 along the a and b axes and 0.00431 along the c axis variations. While the particle size and morphology are quite different. Unlike the previously described 0.3-0.4 μm fibrous particles, the aerinite from the UBC Cliffs is more likely to have an irregular clastic feature with average larger size about 5×10 μm, which may due to weak destruction from short transportation of fluvioglacial sediments. The differences in chemical composition mainly lie in the element content of Ca and Mg. The aerinite from the UBC Cliffs has lower Ca and higher Mg content, which could be caused by different surrounding minerals such as the paragenetic quartz, feldspar, mica and chlorite as well as a small amount of amphibole, and calcite.

5.2 Geochemistry characteristic of the sediments

The Fraser Lowland occupies the Whatcom Basin, where sediments are received since at least the Upper Cretaceous (Rouse et al., 1975). In the Late Tertiary, it has been subjected to considerable tectonic and mountain building activity. During the maximum of the Vashon glaciation in the last Pleistocene, the surrounding area was covered by the thick ice (Mathews et al., 1970). After the ice retreat and the subsequent sea level readjustments from 10000 to 9000 BP, the Fraser River began dumping sediments consisting glacially outwash sands and gravels into the area occupied by the present flood-plain.

According to Clague et al. (1991) , the postglacial deltaic sequence of the Fraser River delta comprises three units (see Fig. 9 left). A few to more than 20 metres thick fine, flat-lying sediments consisting of interbedded mud, sandy silt, and silty fine sand compose the uppermost unit (unit 1), which directly underlies the surface. The topset sequence is underlain by a thick (up to 150 metres) unit (unit 2) consisting mainly of fine to medium sand and silty sand. Unit 2 conformably and gradationally overlies massive, mottled mud and sandy silt of unit 3. The postglacial delta pile overlies a varied suite of Pleistocene sediments (unit P) consisting of mainly mud, silt, and sand. Hebda (1977)'s further study (Fig. 9 right) shows a stratigraphic sequence begins with well-sorted fine silty sands and change to silt with sand lenses in the interval 5.5-5 m. silts continue up to about 4.2 m and then are replaced peats and peat silts, after which peat silts and sands appears at 3.75 m. Then various kinds of peats take over and continue to the surface. Similar to the

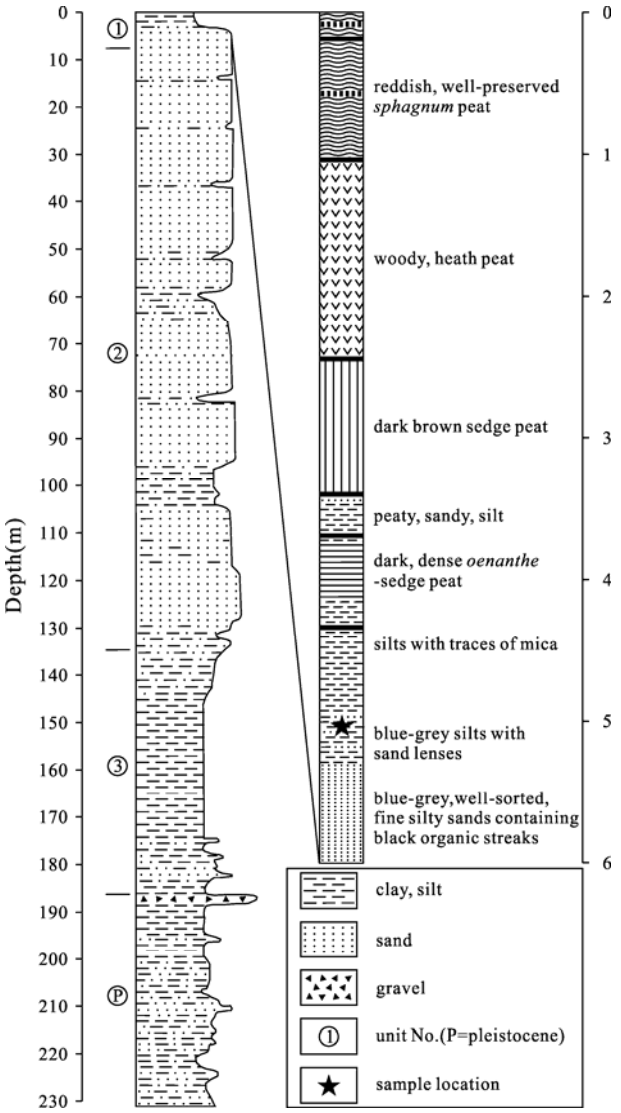

Fig. 9. Lithostratigraphy of a core from the Fraser delta (after Clague et al., 1991 and Hebda, 1977).

Table 5 XRD data of aerinite

Rius et al. (2004)				Observed (this essay)		Calculated (this essay)		
hkl	*d*/nm	2θ/°	I/I_0	*d*/nm	2θ/°	*d*/nm	2θ/°	I/I_0
100	1.46202	6.05	100.00	1.4768	5.98	1.46500	6.03	100.00
300	0.48734	18.20	4.41			0.48840	18.15	3.30
310	0.40549	21.92	16.84	0.4095	21.68	0.40640	21.85	13.80
121	0.37966	23.43	16.36	0.3808	23.34	0.37990	23.40	11.00
400	0.36551	24.35	14.68	0.3654	24.34	0.36603	24.28	5.80
221	0.32832	27.16	9.56	0.3276	27.20	0.32860	27.11	5.30
131	0.32034	27.85	5.27			0.32070	27.80	3.30
410	0.31904	27.97	6.25	0.3189	27.95	0.31980	27.87	3.10
500	0.29240	30.57	2.67			0.29310	30.47	0.90
330	0.28137	31.8	6.21	0.2813	31.78	0.28200	31.70	4.70
411	0.27229	32.89	28.02	0.2721	32.89	0.27270	32.81	14.00
510	0.26259	34.15	3.56	0.2628	34.09	0.26320	34.03	2.30
012	0.25718	34.89	6.52	0.2572	34.86	0.25700	34.88	2.70
112	0.24957	35.99	1.41			0.24940	35.98	0.90
202	0.24602	36.52	1.01	0.2458	36.53	0.24590	36.51	0.50
421	0.24425	36.80	2.94			0.24460	36.71	1.30
430	0.24036	37.42	1.92	0.2403	37.40	0.24090	37.30	1.00
122	0.23619	38.10	3.66	0.2359	38.11	0.23610	38.08	3.30
511	0.23463	38.36	2.52	0.2346	38.34	0.23500	38.27	2.40
302	0.23026	39.12	2.08	0.2302	39.10	0.23020	39.10	1.70
132	0.21962	41.10	3.19			0.21960	41.07	2.00
251	0.21365	42.30	6.98			0.21400	42.19	4.50
042	0.21254	42.53	1.42	0.2126	42.49	0.21260	42.48	0.40
322	0.20611	43.93	2.29			0.20620	43.87	1.60
611	0.20507	44.16	1.74			0.20540	44.05	1.30
412	0.20213	44.84	4.19	0.2018	44.88	0.20220	44.79	1.40
441	0.19567	46.41	1.87	0.1968	46.08	0.19602	46.28	1.00
531	0.19394	46.84	1.46			0.19429	46.71	0.40
332	0.19145	47.49	2.89			0.19155	47.42	1.30
512	0.18520	49.20	1.98	0.1851	49.19	0.18532	49.12	1.20
630	0.18420	49.48	2.61			0.18461	49.32	1.00
800	0.18275	49.90	3.21			0.18316	49.74	1.50
602	0.17819	51.27	1.72	0.1782	51.21	0.17833	51.18	1.10
342	0.17688	51.68	1.45			0.17656	51.73	2.10
522	0.17435	52.48	1.01	0.1747	52.31	0.17449	52.39	0.60
181	0.16262	56.60	1.17			0.16293	56.43	1.00
900	0.16245	56.66	1.89			0.16281	56.47	1.20
551	0.16064	57.36	4.00			0.16096	57.18	2.10
262	0.16017	57.54	1.32			0.16034	57.42	1.00
313	0.16003	57.60	2.44			0.15996	57.57	1.50
143	0.15287	60.57	2.80			0.15284	60.53	1.70
423	0.14734	63.10	1.42			0.14733	63.04	0.70
840	0.13815	67.84	1.45			0.13846	67.60	0.60
092	0.13795	67.95	2.26			0.13815	67.78	1.30
930	0.13516	69.55	1.79			0.13547	69.31	1.10
353	0.13376	70.39	1.21			0.13810	67.80	0.40
014	0.13011	72.67	1.63			0.12999	72.68	0.70
671	0.12591	75.51	1.64			0.12617	75.25	0.80

sand:silt:clay ratio 5.2:78.6:16.2 obtained by Hebda (1977) from sediment collected in the depth of 5.0-5.1 m, our sample was taken from the equivalent layer.

So far as, many indexes appraising the degree of chemical weathering have been proposed and applied, such as Chemical Index of Alteration (CIA, Nesbitt and Young, 1982), Chemical Index of Weathering (CIW, Harnois, 1988) , Plagioclase Index of Alteration (PIA, Fedo et al., 1995), Weathering Index (WIP, Parker, 1970), Index of Compositional Variation (ICV, Cox et al., 1995) , so these indexes are selected to describe chemical weathering intensity in this essay and are expressed as follow respectively:

$CIA=100 \cdot Al_2O_3/(Al_2O_3 + CaO^* + Na_2O + K_2O)$

$CIW=100 \cdot (Al_2O_3/(Al_2O_3 + CaO^* + Na_2O)$

$PIA=100 \cdot (Al_2O_3 - K_2O/(Al_2O_3 + CaO^* + Na_2O - K_2O)$

$WIP=100 \cdot CaO^*/0.7 + 2Na_2O/0.35 + 2K_2O/0.25 + MgO/0.9$

$ICV=(CaO^* + Na_2O + K_2O + Fe_2O_3 + MgO + MnO + TiO_2)/Al_2O$

In formulations above, CaO* represents the Ca fraction in the silicate only, and McLennan (1993)'s theory is used to correct CaO* content.

Chemical analysis shows CIA, CIW, PIA, WIP and ICV are 51, 66, 64, 55 and 0.98, respectively. CIA reflects the degree of aluminosilicate minerals especially feldspar weathering into clay minerals, higher CIA means more Na, K and Ca leach out from silicate minerals, indicating a stronger chemical weathering. On the contrary, higher WIP means lower chemical weathering intensity (Shao and Yang, 2012). According to McLennan (1993), "the average upper crust has a CIA value about 47 and CIA values about 45-55 indicate virtually no weathering". CIW

Table 6 Atomiccoordinates of aerinite

Atom	Occupancy	*x*	*y*	*z*
Ca	0.56	0.337	0.344	0.495
Na	0.44	0.337	0.344	0.495
$Fe^{2+}A$	0.25	0.000	0.000	0.048
$Fe^{3+}A$	0.17	0.000	0.000	0.048
AlA	0.51	0.000	0.000	0.048
MgA	0.07	0.000	0.000	0.048
$Fe^{2+}B$	0.25	0.333	0.667	0.8699
$Fe^{3+}B$	0.17	0.333	0.667	0.8699
AlB	0.51	0.333	0.667	0.8699
MgB	0.07	0.333	0.667	0.870
Al	0.93	0.212	0.333	0.978
Mg	0.07	0.212	0.333	0.978
SiA	1.00	0.202	0.146	0.804
SiB	1.00	0.393	0.521	0.131
O1A	1.00	0.093	0.096	0.802
O2A	1.00	0.248	0.255	0.855
O3A	1.00	0.236	0.133	0.525
O1B	1.00	0.336	0.575	0.119
O2B	1.00	0.329	0.411	0.121
O3B	1.00	0.443	0.535	0.408
O4	0.55	0.578	0.285	0.224
OHA	1.00	0.180	0.270	0.313
OHB	1.00	0.242	0.400	0.654
C	0.55	0.667	0.333	0.224
WatA	1.25	0.419	0.289	0.217
WatB	1.25	0.485	0.379	0.692

R factor of Rietveld refinement is 5.032%

is identical to the CIA by keeping out K_2O from the equation, however, as this approach utilizes total aluminum without considering Al in K-feldspar, it is misleading in K-feldspar–rich rocks for no matter chemically weathered or not, the value is very high. So the use of the CIW calculation to quantify chemical weathering intensity is sometimes inappropriate, and plagioclase weathering PIA should be monitored (Fedo et al., 1995). The PIA equation yields values of 50 for fresh rocks and values close to 100 for clay minerals such as kaolinite, illite, and gibbsite. Another index of compositional variation (ICV) is obtained from the equation of Cox et al. (1995). As clay minerals and nonclay silicate minerals are distinctive in alumina content, this index measures the abundance of alumina relative to the other major cations except for silica in a rock or mineral. As clay minerals contain a higher proportion of Al_2O_3 relative to other nonclay silicates, they have a lower ICV. In addition, among the nonclay silicates, the ICV tends to be highest in minerals such as the pyroxenes and amphiboles, which rank high in the weathering sequence of Goldich (1938), and decreases in more stable minerals such as the alkali feldspars. In our study, the ICV value is 0.97, roughly matched with that of muscovite, illite and plagioclase. As the relationship between resistance to weathering and ICV, the ICV can be applied to mudrocks as a measure of compositional maturity. The values of ICV decrease with increase in the degree of weathering, and it substantiate of a stable condition of the process of chemical weathering. Hence, above index of the sediments reveal near absence of chemical alteration and weak chemical weathering, and consequently might reflect cool and/or arid conditions.

Quartz and feldspar are ubiquitous in sediments, fine grained clay minerals are sensitive to climate changes of depositional environment and geologic process. Since these minerals have undergone virtually no chemical weathering, they show high similarity to those of their provenance, and thus have great significance in the identification of the forming condition and origin of the aerinite.

5.3 Mineral characteristic of the sediments

5.3.1 Quartz and feldspar

Quartz and feldspar are the most common minerals in sediment. During the progress of weathering, quartz is relatively stable, while feldspar is unstable and much easier to be weathered. In consequence, feldspar/quartz ratio (F/Q) , quartz/feldspar ratio (Q/F) or Mineralogical Index of Alteration (MIA=quartz/(quartz + K-feldspar + plagioclase), Perri, 2017) are good indicators to the degree of chemical weathering, thus it is a practical approach to evaluating weathering intensity in clastic sediment, and to speculating sediment provenance as well as climate change (Chen et al., 2015; Yang et al., 2008).

Quartz and feldspar are major components of the UBC Cliffs sediments, whose contents are considerably higher than other minerals. Plagioclase is the main component of feldspar, with An% varying from 30% to 60%, falling in between andesine and labradorite. The F/Q ratios in the

Table 7 Comparison of aerinite from different regions

	Azambre and Monchoux (1988)	Rius et al. (2004)	Rius et al. (2009)	This essay
Location	St.Pandelon, France	Huesca, Spain	Catalunya, Spain	the UBC Cliffs, Canada
Geologic Setting	Formed by alteration of ophitic rocks from the upper Triassic of the Pyrenees, associated with calcite, quartz, andplagioclase etc. Appear as earthy, pale-blue masses or silky, bright to pale blue fibres with diameters up to the 0.3–0.4 μm range			Fluvioglacial sediments in paragenetic with quartz, feldspar, mica and chlorite Irregular clastic particles in size of about 5×10 μm
Crystal Structure	*a*=1.4690 nm *b*=1.6872 nm *c*=1.5170 nm *β*=94.45° *V*=1.277 nm^3	*a*=*b*=1.68820(9) nm *c*=0.52251(3) nm *V*=1.2897(1)nm^3 *P*3*c*1	*a*=*b* =1.69161(1) nm *c*=0.52289(1) nm *V*=1.296 nm^3 *P*3*c*1	*a*=*b*=1.692(5) nm *c*=0.5220(32) nm *V*=1.294 nm^3 *P*3*c*1
Chemical Composition	$(Ca_{4.0}Na_{0.2})$ $(Fe^{3+}{}_{1.7}Fe^{2+}{}_{0.9}Mg_{1.5}Al_{6.1})$ $(Si_{11.6}P_{0.2}Al_{0.3})\ O_{36}(OH)_{12}\cdot$ $12H_2O + CO_2$	$(Ca_{5.1}Na_{0.5})$ $(Fe^{3+}AlFe^{2+}{}_{1.7}Mg_{0.3})$ $(Al_{5.1}Mg_{0.7})$ $[Si_{12}O_{36}(OH)_{12}H]$ $[(CO_3)_{1.2}(H_2O)_{12}]$	$(Ca_{4.31}Na_{0.07})$ $(Al_{5.25}Si_{0.43}Mg_{0.33})$ $(Fe^{3+}{}_{1.36}Fe^{2.5+}{}_{0.64})$ $(Fe^{3+}{}_{1.2}Mg_{0.5}Al_{0.3})$ $[Si_{12}O_{36}(OH)_{12}]$ $[(CO_3)_{0.75}(SO_3)_{0.25}(H_2O)_{11.1}]$	$(Mg_{3.06}Ca_{0.36}Na_{0.63}\ K_{0.75})_{4.8}$ $(Fe^{3+}{}_{2.67}Fe^{2+}{}_{1.80}Mg_{0.38}Al_{5.09}$ $Mn^{2+}{}_{0.04}Cr^{3+}{}_{0.01}Ni^{2+}{}_{0.01})_{10}$ $(Si_{11.63}Ti_{0.37})_{12}\,O_{36}(OH)_{12}\cdot$ $12H_2O + CO_2$

whole rock sample, Aer-1, Aer-2 and Aer-3 are 9.72, 15.54, 10.70 and 10.44, respectively. Above data show much higher content of feldspar over quartz, indicating that the sediments have undergone weak and low degree weathering.

5.3.2 Muscovite

Illite, one of the most widely distributed clay minerals in nature, is an important index mineral in paleoclimatic study (An et al., 2018; Hu and Yu, 2017; Wang and Zhou, 1998). Griffin et al. (1968) conducted a research on the distribution of marine clays in the world, and figured out that the northern ocean has more illite than the southern counterparts, which clearly reflects continental input. In addition, on the basis of age or geographical distribution, there is no evidence for illite formation in situ in the marine environment. Generally, illite can remain stable under cold and dry climate condition (Chen and Wang, 2007; Chen et al., 2005). In low temperature or in humid and alkalescent conditions, feldspar and mica lose potassium to form illite, while with interlayer space continuously loses potassium and absorbs magnesium under alkaline condition illite turn into montmorillonite or mixed-layer illite. If the climate gets more torrid and humid, chemical weathering reinforces, taking away massive potassium and leading to illite decomposing into kaolinite and eventually laterization (Wu et al., 2007). Hence dry climate with weak eluviation is beneficial to the formation and preservation of illite.

The appearance of mica and absence of kaolinite and montmorillonite (kaolinite and montmorillonite prefer moist and mild conditions) demonstrate the weak chemical weathering and hydrolysis of the UBC Cliffs sediments. It is known from the EDS (SEM) results that the interlayer cation varying from about 0.6 to 0.85 (Table 3)(Wang et al., 2007), roughly match that of illite. Moreover, the mica and chlorite assemblage reveals felsic parent rock and relatively arid condition with weak chemical weathering and strong physical weathering. In warm and moist climate it is prone to weather into kaolinite, montmorillonite, mixed-layer minerals and other clay minerals. Mica, quartz and feldspar paragenetic assemblage indicates the high debris input in arid climate (Garzanti et al., 2014) .

Esquevin (1969) proposed a Chemical Index (CI) to measure the intensity of weathering, which shows the weathering degree of the parent rocks and reveals the climate change of the provenance (Ehrmann, 1998; Kong et al., 2011; Liu et al., 2007). If the area ratio of 0.5 nm /1 nm EG saturated XRD diffraction peaks (in this paper 0.2) is greater than 0.5, it means an intense hydrolysis, otherwise, it means principally physical weathering is functioning or physical weathering is stronger than chemical weathering (Esquevin, 1969; Gingele, 1996).

5.3.3 Chlorite

Chlorite is a common mineral in clastic rocks (and sediments) including low temperature metamorphic, diagenetic and sedimentary rocks (sediments), which is of detrital and authigenic origins. Usually chlorite is preserved in places where chemical weathering is restrained and chemical destruction is absent (e.g. arid and glacier surface, high latitude area especially polar region), because chlorite is easy to weather into montmorillonite, mixed-layer minerals and other clay minerals(Li et al., 2012). Chlorite is an indicator of low intensity weathering process on land and perhaps a fluvioglacial transport (Chen et al., 2005; Griffin et al., 1968).

Chlorite is preserved in the UBC Cliffs because of the high latitude and the cold weather condition. From EDS (SEM) data, chlorite here is rich in iron, in accordance with Mackintosh and Gardner (1966)'s study on west coast of the Fraser River that chlorite rich in iron and manganese adapts better in such cold and dry environments. The preservation and accumulation of illite and chlorite assemblage after periodic erosion declare the physical weathering rather than chemical one.

Contrast with Griffin et al. (1968)'s state "there is about equal amounts of montmorillonite, chlorite and illite in the Fraser River", no montmorillonite or mixed-layer mineral is found in the studied specimens. This may be explained by Whitehouse and McCarter (1956)'s research that montmorillonite can transform into illite and chlorite in artificial sea water under the influence of inorganic ions, while no evidence shows illite or kaolinite transformation into other clays. However, whether or not the conversion can happen in real sea water remains unclear.

6 Conclusions

(1) Aerinite is identified in the pale blue outcrop from the UBC Cliffs, and the composition and structure characteristics of the sediments are summarized.

(2) Aerinite is found in a high latitude area and in paragenetic with quartz, feldspar, mica and chlorite as well as a small amount of amphibole, calcite, clinopyroxene, rutile, perovskite and apatite.

(3) Mineralogical and geochemistry characteristics (CIA, CIW, PIA, WIP and ICV) indicate that aerinite and these minerals are adapted to high latitude and cold dry climate. These minerals show high similarity to those from their origin, thus they have great significance in the identification of the forming condition and origin of the aerinite.

Acknowledgements

This work is supported by the National Natural Sciences Foundation of China [Grant No: 41872048, 41372061, 40972038]. Guanyu Wang is grateful for the financial support from China Scholarship Council (No 201806010080) and technical support from Jianguo Wen and Seungyeol Lee.

Manuscript received Aug. 1, 2019
accepted Dec. 20, 2019
associate EIC FEI Hongcai
edited by LIU Lian

References

Amos, C., Feeney, T., Sutherland, T., and Luternauer, J., 1997. The stability of fine-grained sediments from the Fraser River Delta. Estuarine, Coastal and Shelf Science, 45(4): 507–524.

An, J.L., Wang, H.J., and Yuan, L., 2018. Very low-grade metamorphism of the Precambrian along profile Kaili-Rongjiang Congjiang in southeastern Guizhou Province, China. Acta Petrologica Sinica, 34(3): 669–684 (in Chinese with English abstract).

Armstrong, J.E., and Clague, J., 1977. Two major Wisconsin lithostratigraphic units in southwest British Columbia. Canadian Journal of Earth Sciences, 14(7): 1471–1480.

Armstrong, J.E., Crandell, D.R., Easterbrook, D.J., and Noble, J., 1965. Late Pleistocene stratigraphy and chronology in southwestern British Columbia and northwestern Washington. Geological Society of America Bulletin, 76(3): 321–330.

Attard, M.E., Venditti, J.G., and Church, M., 2014. Suspended sediment transport in Fraser River at Mission, British Columbia: New observations and comparison to historical records. Canadian Water Resources Journal/Revue canadienne des ressources hydriques, 39(3): 356–371.

Azambre, B., and Monchoux, P., 1988. Précisions minéralogiques sur l'aérinite: nouvelle occurrence à Saint-Pandelon (Landes, France). Bulletin de minéralogie, 111(1): 39–47.

Casas, A.P., and Llopis, J.d.A., 1992. The identification of aerinite as a blue pigment in the Romanesque frescoes of the Pyrenean region. Studies in Conservation, 37(2): 132–136.

Chen, J.J., Hong, H.L., Liu, Z., Song, E.P., Wang, C.W., Jiang, G.L., Yin, K., and Zhang, K.X., 2015. Mineral assemblage characteristics of the Oligocene Miocene sediments in the Gerze Basin, Tibet, and their paleoclimatic significance. Acta Petrologica Et Mineralogica, 34(3): 393–404 (in Chinese with English abstract).

Chen, T., and Wang, H.J., 2007. Science in China Series D-Earth Sciences, 37(7): 894–899 (in Chinese).

Chen, T., Wang, H.J., Zhang, Z.Q., and Wang, H., 2005. An approach to paleoclimate-reconstruction by clay minerals. Acta Acientiarum Naturalium, Universitatis Pekinensis, 41(2): 309–316 (in Chinese with English abstract).

Clague, J.J., 1976. Quadra Sand and its relation to the late Wisconsin glaciation of southwest British Columbia. Canadian Journal of Earth Sciences, 13(6): 803–815.

Clague, J.J., 1977. Quadra Sand: a study of the Late Pleistocene geology and geomorphic history of coastal southwest British Columbia. Geological Survey of Canada, 77–17.

Clague, J.J., and Bornhold, B.D., 1980. Morphology and littoral processes of the Pacific coast of Canada. The Coastline of Canada, Geological Survey of Canada, 80–10.

Clague, J.J., Froese, D., Hutchinson, I., James, T.S., and Simon, K.M., 2005. Early growth of the last Cordilleran ice sheet deduced from glacio-isostatic depression in southwest British Columbia, Canada. Quaternary Research, 63(1): 53–59.

Clague, J.J., Luternauer, J., Pullan, S., and Hunter, J., 1991. Postglacial deltaic sediments, southern Fraser River delta, British Columbia. Canadian Journal of Earth Sciences, 28(9): 1386–1393.

Clague, J.J., Luternauer, J.L., and Hebda, R.J., 1983. Sedimentary environments and postglacial history of the Fraser Delta and lower Fraser Valley, British Columbia. Canadian Journal of Earth Sciences, 20(8): 1314–1326.

Clark, R.J., Hark, R.R., Salvadó, N., Butí, S., and Pradell, T., 2010. Spectroscopy study of mural paintings from the Pyrenean Church of Saint Eulàlia of Unha. Journal of Raman Spectroscopy, 41(11): 1418–1424.

Cox, R., Lowe, D.R., and Cullers, R., 1995. The influence of sediment recycling and basement composition on evolution of mudrock chemistry in the southwestern United States. Geochimica et Cosmochimica Acta, 59(14): 2919–2940.

Daniel, F., Mounier, A., and Laborde, B., 2008. Pigment aerinite as a sign of artist circulation through Pyreneas in the mediaeval period. In: Proceedings, V Congresso Nazionale di Archeometria "Scienza e Beni Culturali", Syracuse, 26–29.

Ehrmann, W., 1998. Implications of late Eocene to early Miocene clay mineral assemblages in McMurdo Sound (Ross Sea, Antarctica) on paleoclimate and ice dynamics. Palaeogeography, Palaeoclimatology, Palaeoecology, 139(3–4): 213–231.

Esquevin, J., 1969. Influence de la composition chimique des illites sur leur cristallinité. Bull. Centre Rech. Pau-SNPA, 3 (1): 147–153.

Fedo, C.M., Wayne Nesbitt, H., and Young, G.M., 1995. Unraveling the effects of potassium metasomatism in sedimentary rocks and paleosols, with implications for paleoweathering conditions and provenance. Geology, 23(10): 921–924.

Folk, R.L., Andrews, P.B., and Lewis, D., 1970. Detrital sedimentary rock classification and nomenclature for use in New Zealand. New Zealand journal of geology and geophysics, 13(4): 937–968.

Frost, R.L., Scholz, R., and López, A., 2015. Infrared and Raman spectroscopic characterization of the carbonate bearing silicate mineral aerinite–Implications for the molecular structure. Journal of Molecular Structure, 1097: 1–5.

Garrison, R.E., Luternauer, J.L., Grill, E.V., MacDonald, R.D., and Murray, J.W., 1969. Early diagenetic cementation of recent sands, Fraser River delta, British Columbia. Sedimentology, 12(1–2): 27–46.

Garzanti, E., Padoan, M., Setti, M., López-Galindo, A., and Villa, I.M., 2014. Provenance versus weathering control on the composition of tropical river mud (southern Africa). Chemical Geology, 366: 61–74.

Gingele, F.X., 1996. Holocene climatic optimum in Southwest Africa—evidence from the marine clay mineral record. Palaeogeography, Palaeoclimatology, Palaeoecology, 122(1–4): 77–87.

Goldich, S.S., 1938. A study in rock-weathering. The Journal of Geology, 46(1): 17–58.Griffin, J.J., Windom, H., and Goldberg, E.D., 1968. The distribution of clay minerals in the world ocean. In: Proceedings, Deep Sea Research and Oceanographic Abstracts, Vol. 15, Elsevier, 433–459.

Groth, P., 1898. Tabellarische Übersicht der Mineralien. Braunschweig: Friedrich & Sohn Verlag, 1–138.

Harnois, L., 1988. The CIW index: a new chemical index of weathering. Sedimentary geology, 55: 319–322.

Hart, B.S., Hamilton, T.S., and Barrie, J.V., 1998. Sedimentation rates and patterns on a deep-water delta (Fraser Delta, Canada); integration of high-resolution seismic stratigraphy, core lithofacies, and 137 Cs fallout stratigraphy. Journal of Sedimentary Research, 68(4): 556–568.

Hebda, R.J., 1977, The paleoecology of a raised bog and associated deltaic sediments of the Fraser River delta (Ph. D thesis). University of British Columbia, 1–203.

Hu, D.Q., and Yu, J.J., 2017. Study of illite in the Upper Paleozoic, in northeastern Inner Mongolia. Acta Petrologica Sinica, 25(8): 2017–2022 (in Chinese with English abstract).

Ibáñez-Insa, J., Oriols, N., Elvira, J.J., Álvarez, S., and Plana, F., 2012. Heat alteration of the blue pigment aerinite: Application to Sixena's Romanesque frescoes. Macla, 12: 46–47.

Jena, P., and Mishra, P., 2017. Microstructural, Raman, EPMA and X-ray Tomographic Study of the Odisha's Beryl. (Emerald) Sample. J Geol Geophys, 6(288): 2–4.

Kong, W.L., Li, S.Y., Wan, Q., Du, Y.L., and Wang, S., 2011. Differentiation and discrimination of marine clay minerals as indicators of paleoenvironment. Journal of Anhui University (Natural Science Edition), 35(5): 100–108 (in Chinese with English abstract).

La Croix, A.D., and Dashtgard, S.E., 2015. A synthesis of depositional trends in intertidal and upper subtidal sediments across the tidal–fluvial transition in the Fraser River, Canada. Journal of Sedimentary Research, 85(6): 683–698.

Li, C.S., Shi, X.F., Gao, S.J., Chen, M.D., Liu, Y.G., Fang, X.S., Lv, H.H., Zou, J., J, Liu, S.F., and Qiao, S.Q., 2012. Clay mineral composition and their sources for the fluvial sediments of Taiwanese rivers. Chinese Science Bulletin, 57 (6): 673–681 (in Chinese with English abstract).

Li, X.L., Zhang, L.F., Wei, C.J., and Zhang, G.B., 2017. Application of Zr-in-rutile thermometry and its interpretation on the Archean eclogite from Belomorian province, Russia. Acta Petrologica Sinica, 33(10): 3263–3277 (in Chinese with English abstract).

Lintern, D.G., Hill, P.R., and Stacey, C., 2016. Powerful unconfined turbidity current captured by cabled observatory on the Fraser River delta slope, British Columbia, Canada.

Sedimentology, 63(5): 1041–1064.
Liu, Z.F., Zhao, Y.L., Li, J.R., and Colin, C., 2007. Science in China Series D-Earth Sciences, 37(9): 1176–1185 (in Chinese).
Lu, L.N., Li, J., Yang, M., and Zheng, C.J., 2016. Mineralogy Analysis of Granites in Diaoyutai Area of Western Liaoning Province. DEStech Transactions on Engineering and Technology Research (mcee), 17–20.
Luternauer, J., 1980. Genesis of morphologic features on the western delta front of the Fraser River, British Columbia—status of knowledge. The Coastline of Canada, 381–396.
Mackintosh, E.E., and Gardner, E., 1966. A mineralogical and chemical study of lower Fraser River alluvial sediments. Canadian Journal of Soil Science, 46(1): 37–46.
Mathewes, R.W., 1979. A paleoecological analysis of Quadra Sand at Point Grey, British Columbia, based on indicator pollen. Canadian Journal of Earth Sciences, 16(4): 847–858.
Mathews, W.H., Fyles, J., and Nasmith, H., 1970. Postglacial crustal movements in southwestern British Columbia and adjacent Washington State. Canadian Journal of Earth Sciences, 7(2): 690–702.
McLennan, S.M., 1993. Weathering and global denudation. The Journal of Geology, 101(2): 295–303.
McManus, J., 1988. Grain size determination and interpretation. Techniques, in sedimentology, 63–85.
Nesbitt, H.W., and Young, G.M., 1982. Early Proterozoic climates and plate motions inferred from major element chemistry of lutites. Nature, 299(5885): 715–717.
Parker, A., 1970. An index of weathering for silicate rocks. Geological Magazine, 107(6): 501–504.
Pérez-Arantegui, J., Pardos, C., Abad, J.-L., and García, J.-R., 2013. Microcharacterization of a natural blue pigment used in wall paintings during the Romanesque period in northern Spain. Microscopy and Microanalysis, 19(6): 1645–1652.
Perri, F., 2017. Reconstructing chemical weathering during the Lower Mesozoic in the Western-Central Mediterranean area: a review of geochemical proxies. Geological Magazine, 155(4): 944–954.
Rius, J., Crespi, A., Roig, A., and Melgarejo, J.C., 2009. Crystal-structure refinement of Fe3 +-rich aerinite from synchrotron powder diffraction and Mössbauer data. European Journal of Mineralogy, 21(1): 233–240.
Rius, J., Elkaim, E., and Torrelles, X., 2004. Structure determination of the blue mineral pigment aerinite from synchrotron powder diffraction data: The solution of an old riddle. European Journal of Mineralogy, 16(1): 127–134.
Rouse, G., Mathews, W., and Blunden, R., 1975. The Lions Gate Member: A New Late Cretaceous Sedimentary Subdivision in the Vancouver Area of British Columbia. Canadian Journal of Earth Sciences, 12(3): 464–471.
Ryder, J., Fulton, R., and Clague, J., 1991. The Cordilleran ice sheet and the glacial geomorphology of southern and central British Colombia. Géographie physique et Quaternaire, 45(3): 365–377.
Salvadó, N., Butí, S., Pantos, E., Bahrami, F., Labrador, A., and Pradell, T., 2008. The use of combined synchrotron radiation micro FT-IR and XRD for the characterization of Romanesque wall paintings. Applied Physics A, 90(1): 67–73.
Shao, J.Q., and Yang, S.Y., 2012. Does chemical index of alteration (CIA) reflect silicate weathering and monsoonal climate in the Changjiang River basin? Chinese science bulletin, 57(11): 933–942 (in Chinese with English abstract).
Silva, J.C.R., 1996. Blue quartz from the Antequera-Olvera ophite, Malaga, Spain. The mineralogical Record, 27(2): 99–104.
Von Lasaulx, A., 1876. Aërinit, ein neues Mineral. N. Jb. Mineral, 175: 352–358.
Wang, H.J., Tao, X.F., and Rahn, M., 2007. Some aspects of illite crystallinity and its applications in low temperature metamorphism. Earth Science Frontiers, 14(1): 151–156 (in Chinese with English abstract).
Wang, H.J., and Zhou, J., 1998. On the indices of illite crystallinity. Acta Petrologica Sinica, 14(3): 395–405 (in Chinese with English abstract).
Wang, H.J., Zhou, J., Xu, Q.S., Liu, C.X., and Zhu, M.X., 2002. Science in China Series D-Earth Sciences, 32(9): 742–750 (in Chinese).
Wang, H.J., Zhou, Z., Wang, L., and Yuan, L., 2014. Anchimetamorphism and diagenesis of the Meso-Neoproterozoic and the Lower Paleozoic along profile Yangjiaping in North Hunan Province, China. Acta Petrologica Sinica, 30(10): 3013–3020 (in Chinese with English abstract).
Wentworth, C.K., 1922. A Scale of Grade and Class Terms for Clastic Sediments. Journal of Geology, 30(5): 377–392.
Whitehouse, U.G., and McCarter, R.S., 1956. Diagenetic modification of clay mineral types in artificial sea water. Clays and clay minerals, 5(1): 81–119.
Wu, M., Li, S.R., Chu, F.Y., Long, J.P., and Tan, W.H., 2007. The assemblage and environmental significance of clay minerals in the surface sediments around Hainan Island. Journal of Mineralogy and Petrology, 27(2): 101–107 (in Chinese with English abstract).
Yang, Z.S., Zhao, X.H., Qiao, S.Q., Li, Y.H., and Fan, D.J., 2008. Feldspar/Quartz (F/Q) Ratios as a Chemical Weathering Intensity Indicator in Different Grain Size-Fractions of Sediments from the Changjiang and Huanghe Rivers to the Seas. Periodical of Ocean University of China, 38(2): 244–250 (in Chinese with English abstract).
Yin, K.D., Zetsche, E.M., and Harrison, P.J., 2016. Effects of sandy vs muddy sediments on the vertical distribution of microphytobenthos in intertidal flats of the Fraser River Estuary, Canada. Environmental Science & Pollution Research International, 23(14): 14196–14209.

About the author

WANG Guanyu, female, born in 1992, PhD Candidate of Peking University, clay minerals. Email: gywang@pku.edu.cn.

About the corresponding author

WANG Hejing, male, born in 1958, doctor, clay minerals, School of Earth and Space Sciences, Peking University, professor.